JACS
JOURNAL OF THE AMERICAN CHEMICAL SOCIETY

ARTICLE

pubs.acs.org/JACS

Magnetic Nanoparticles-Templated Assembly of Protein Subunits: A New Platform for Carbohydrate-Based MRI Nanoprobes

Elsa Valero,[†] Stefano Tambalo,[‡] Pasquina Marzola,[‡] Mariano Ortega-Muñoz,[§] F. Javier López-Jaramillo,[§] Francisco Santoyo-González,[§] Juan de Dios López,[∥] Juan J. Delgado,[∥] José J. Calvino,[∥] Rafael Cuesta,[⊥] José M. Domínguez-Vera,*[,†] and Natividad Gálvez*[,†]

[†]Departamento de Química Inorgánica, Universidad de Granada, 18071 Granada, Spain

[‡]Dipartimento di Informatica, Università degli Studi di Verona, Italy

[§]Departamento de Química Orgánica, Instituto de Biotecnología, Universidad de Granada, Avda. Fuentenueva s/n, 18071 Granada, Spain

[∥]Departamento Ciencia de Materiales e Ingeniería Metalúrgica y Química Inorgánica, Universidad de Cádiz, Campus Río San Pedro, 11510 Cádiz, Spain

[⊥]Departamento de Química Inorgánica y Orgánica, EPS Linares, Universidad de Jaén, 23700 Linares, Spain

Supporting Information

ABSTRACT: A new approach for the preparation of carbohydrate-coated magnetic nanoparticles is reported. In a first step, we show that the pH-driven assembly-disassembly natural process that occurs in apoferritin protein is effective for the encapsulation of maghemite nanoparticles of different sizes: 4 and 6 nm. In a second step, we demonstrate that the presence of functional amine groups in the outer shell of apoferritin allows functionalization with two carbohydrates, *N*-acetyl-D-glucosamine and D-mannose. High-resolution electron microscopy (HREM), high angle annular dark field scanning electron microscopy (HAADF-STEM), electron energy loss spectroscopy (EELS), X-ray diffraction (XRD), and SQUID technique have been used to characterize the magnetic samples, termed herein Apomaghemites. The in vivo magnetic resonance imaging (MRI) studies showed the efficiency in contrasting images for these samples; that is, the r_2 NMR relaxivities are comparable with Endorem (a commercial superparamagnetic MRI contrast agent). The r_2 relaxivity values as well as the pre-contrast and post-contrast T_2*-weighted images suggested that our systems could be used as perspective superparamagnetic contrast agents for magnetic resonance imaging (MRI). The carbohydrate-functionalized Apomaghemite nanoparticles retained their recognition abilities, as demonstrated by the strong affinity with their corresponding carbohydrate-binding lectins.

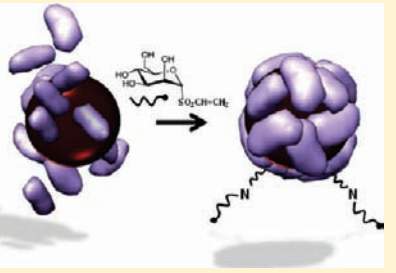

INTRODUCTION

In the past few years, we have witnessed an enormous development in the synthesis and functionalization of inorganic nanoparticles for biomedical applications. Of particular interest is the case of magnetic nanoparticles where there is an outbreak of proposed nanostructures for magnetic resonance imaging (MRI), magnetic hyperthermia, or targeted drug delivery.[1]

Magnetite and/or maghemite (Fe_3O_4/γ-Fe_2O_3) nanoparticles have been used extensively as a model of magnetic material in the biomedical research field.[2] In particular, water-soluble magnetic iron oxides, which are coated with biocompatible polymers, serve as contrast agents for MRI nowadays.[3] However, when using these iron oxide nanoparticles in biomedical applications, it is crucial to control their size monodispersity, degree of aggregation, magnetic properties (high saturation magnetization (M_s) values while maintaining single domain properties), and their ability to target specific cells and/or tissues.

An extremely efficient method to obtain non-aggregated, size-controlled magnetic nanoparticles is the use of a preorganized matrix as a chemical and spatial nanocage where the nanoparticles are formed. Typical examples of molecular nanocages have been proteins, specifically apo- and apoferritin-like proteins.[4] The virus capsids are also an appealing system; their templated self-assembly around different types of inorganic nanoparticles has been demonstrated by Dragnea's group.[5] In this context, the pH-driven disassembly−assembly process occurring in multimeric apoferritin is a feasible approach to encapsulate small molecules.[6] Recently, the salt-mediated assembly of the hyperthermophile Archaeoglobus fulgidus ferritin around 10 nm gold nanoparticles has been reported.[7]

Additionally, numerous efforts are being devoted to achieve "active targeting", that is, ligand-coated nanoparticles bearing an active functionality, such as a targeting molecule for a desired receptor.[8]

Among ligands for specific targeting, saccharides are promising molecules because they act as recognition markers in numerous biological processes.[8] Their presence on cell surfaces

Received: November 8, 2010
Published: March 08, 2011

Scheme 1. Schematic Encapsulation of Maghemite Nanoparticles Thanks to the pH-Driven Disassembly−Assembly Process Exhibited in Apoferritin

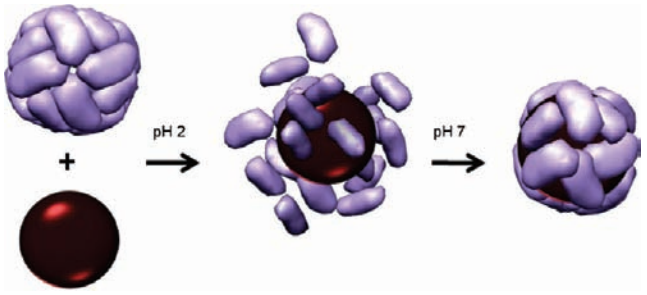

may be recognized by carbohydrate-binding proteins such as antibodies, enzymes, or lectins; the latter bind to mono- and oligosaccharides with high specificity.[9] Numerous examples of magnetic nanoparticles coated with polysaccharides or biocompatible polymers (dextran, albumin, etc.) have also been announced.[3] However, there are only a few examples of nanoparticles functionalized with biologically significant oligosaccharides, where the saccharides truly confer a new biological functionality to the inorganic nanoparticle and not a simple stabilizing role.[10]

In this Article ,we describe a new synthetic method for obtaining carbohydrate-functionalized magnetic nanoparticles based on the pH-driven disassembly/assembly of horse spleen apoferritin. To our knowledge, this is the first example of both a templated self-assembly of apoferritin around maghemite nanoparticles and its conversion into a glycosylated specimen.

RESULTS AND DISCUSSION

In a first step, magnetite nanoparticles were prepared by coprecipitation of iron salts in water. As compared to non-polar organometallic routes,[11] aqueous syntheses are more reproducible, cheaper, and non-toxic, and the as-prepared samples have high aqueous stability and biological compatibility. Besides, magnetite nanoparticles obtained in organic solvents are usually stabilized by hydrophobic non-degradable surfactants and have the problem of replacing these surfactants by hydrophilic ones. The aqueous coprecipitation method allows one to tune the size of magnetite nanoparticles by controlling the pH and ionic strength of the synthetic medium, as was previously reported.[12] We synthesized magnetite nanoparticles of 4 and 6 nm on average size. Oxidation of magnetite in acidic conditions resulted in a colloid of maghemite (γ-Fe_2O_3) nanoparticles, which are chemically stable at pH 2.[13]

In a second step, the acidic colloid of maghemite nanoparticles was incubated with disassembled apoferritin at pH 2, and then the protein was reassembled by increasing the pH at 7, entrapping the nanoparticles inside the cavity (Scheme 1). At pH 2, the apoferritin is dissociated into its 24 polypeptide subunits, and the increase of the pH up to pH 7 produces the reassembly of subunits. We obtained water-soluble, size-controlled magnetic bionanoparticles thanks to this synthetic approach. In a control experiment, without protein, precipitation of maghemite nanoparticles occurs.

The presence of magnetic iron oxide nanoparticles serves as a template for the protein to self-assemble. The 4 nm sample will be named herein APOMAG-4 and the 6 nm sample APOMAG-6.

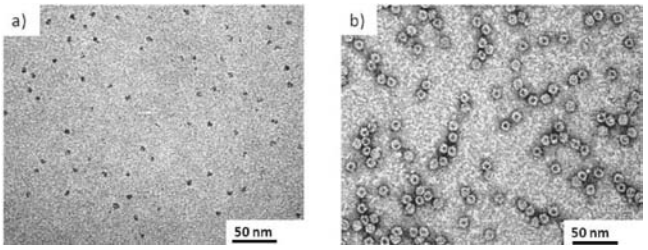

Figure 1. (a) TEM image of APOMAG-4; and (b) uranyl negative stained of (a). Similar images were obtained for the APOMAG-6 sample (data not shown).

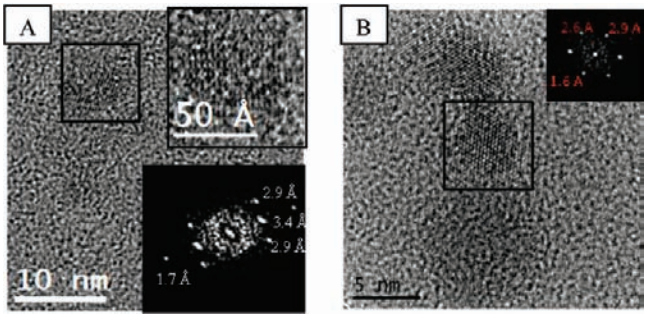

Figure 2. (A) HREM image of APOMAG-4. The black square shows a nanoparticle. Inset: DDP of the selected particle. (B) Same as (A) for the APOMGA-6 sample.

As an advantage over previous reported works for the in situ synthesis of magnetite inside the apoferritin, we used a stable colloid of pre-formed maghemite nanoparticles that does not evolve chemically and prevents the eventual precipitation of material outside the protein.[14]

The purification of the system was carried out by size exclusion chromatography (Supporting Information SI1). The fractions containing protein and magnetic nanoparticles were isolated and studied by transmission electron microscopy (TEM), high angle annular dark field scanning electron microscopy (HAADF-STEM), electron energy loss spectroscopy (EELS), X-ray diffraction (XRD), SQUID technique, relaxivity measurements, and MRI in vivo experiments.

TEM images of magnetic colloids mainly showed irregular spherical nanoparticles (SI2). As expected, maghemite nanoparticles are found more isolated when encapsulated by apoferritin, as observed in Figure 1a. The protein shell was visualized by negative staining with uranyl acetate, confirming that the nanoparticles were actually encapsulated within the apoferritin shell (Figure 1b). Numerical analysis of the images showed a 75% of successful encapsulation. Negative staining of the samples at pH 2 revealed the dissociated state (i.e., non-assembly) of the protein (data not shown).

The average particle size and standard deviation were estimated from the HAADF-STEM images (Supporting Information SI4). The mean particle sizes were 4.2 ± 0.2 and 6.5 ± 0.2 nm for the APOMAG-4 and APOMAG-6, respectively.

Figure 2 shows high-resolution electron microscopy (HREM) images for both Apomaghemite samples. The digital diffraction pattern (DDP) of one particle clearly shows eight spots that correspond to four families of equivalent crystallographic planes. An in-depth analysis of the DDP using the Z-Axe software[15]

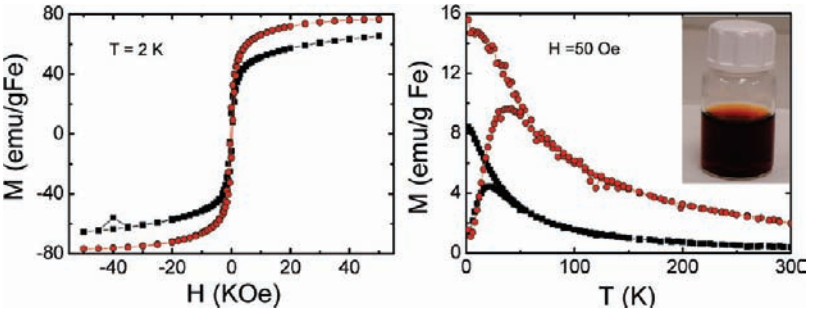

Figure 3. (a) Hysteresis loops of APOMAG-4 (■) and APOMAG-6 (red ●) samples at $T = 2$ K; and (b) zero field cooled-field cooled curves registered at a field (H) of 50 Oe. Inset: APOMAG-4 sample.

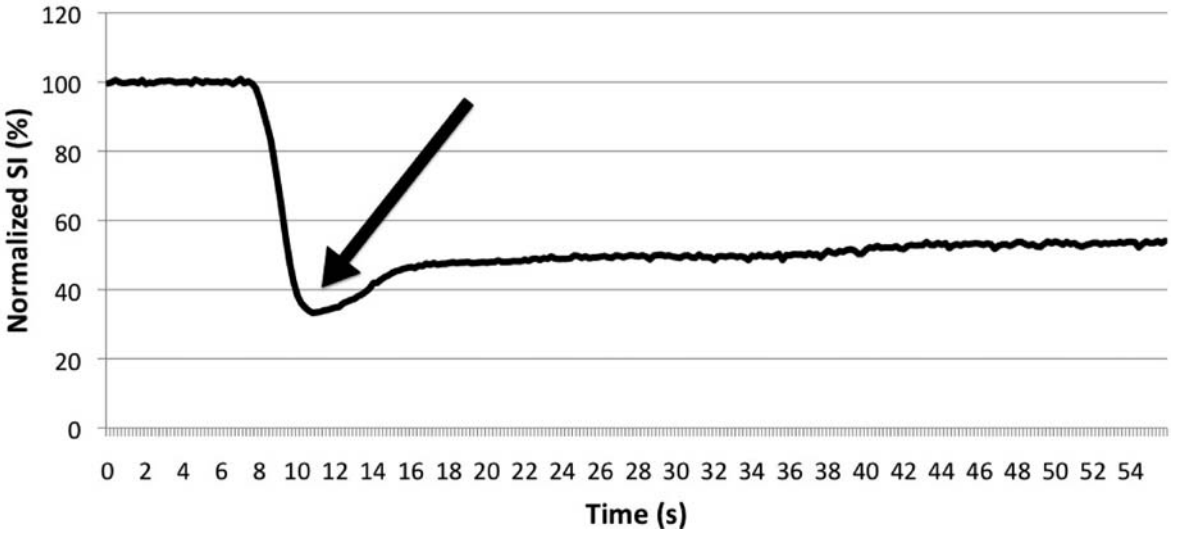

Figure 4. Representative first passage curve obtained using APOMAG-6. The arrow indicates the time point of maximum signal drop.

indicated that the calculated *d*-spacing and angles can only be interpreted considering the following structures: magnetite or maghemite. Besides, dynamic diffraction pattern and image simulation of the different possible phases in the adequate orientation suggested that the most suitable phases were magnetite and maghemite. Some electron energy loss spectra (EELS) for both Apomaghemite samples are included in Supporting Information SI4, showing that apart from maghemite we cannot exclude the presence of a small quantity of magnetite.

X-ray diffraction (XRD) measurements of the magnetic colloids also showed typical XRD patterns for maghemite and/or magnetite spinel oxides (Supporting Information SI3).[12] On the basis of the calculations with the Debye−Scherrer's formula, the mean grain sizes of maghemites were 3.8 and 6.5 nm for APOMAG-4 and APOMAG-6, respectively, consistent with HAADF-STEM measurements.

Before using the Apomaghemite nanoplatform for biological tests, we examined their magnetic properties by the SQUID technique (Figure 3). [16] Zero field cooled-field cooled (ZFC-FC) magnetization curves were performed as a function of temperature (2−300 K) at a field of H = 50 Oe (Figure 3b). The obtained blocking temperatures (T_B) were 20 and 35 K for APOMAG-4 and APOMAG-6, respectively. Above T_B, ZFC and FC curves superimpose perfectly, so we can rule out the presence of much aggregation. It is relevant to note that the obtained T_B values were comparable to that of γ-Fe_2O_3 nanoparticles of the same size.[16,17]

Table 1. Maximum Signal Drop (Average ± Standard Deviation) in First Passage Curves for APOMAG-4, APOMAG-6, and Endorem[a]

	normalized SI (%)
APOMAG-4	70.5 ± 9.8
APOMAG-6	76.5 ± 7.2
Endorem	73.6 ± 4.1

[a] Values of SI are normalized as described in the text.

Figure 3a shows the hysteresis loops recorded at 2 K, that is, below the blocking temperature. The particles showed ferrimagnetic behavior at this temperature. The magnetization (M) curves measured versus applied fields (H) reflect the particle anisotropy. The coercivity (H_c) was 336 Oe for APOMAG-4 and 340 Oe for APOMAG-6, and the mass magnetization (M_S) was 64 and 76 emu/g Fe for APOMAG-4 and APOMAG-6, respectively, in agreement with values reported previously for the same size and nanomaterial.[17] Magnetization recorded at 300 K did not show coercive field or remanence magnetization, characteristics of a superparamagnetic regime.

MRI is one of the most powerful noninvasive techniques for the diagnosis of many diseases in human soft tissues. We tested the efficiency in contrasting MRI images of the Apomaghemite samples. In MRI, the contrast enhancement effects are directly related to the relaxivity value of the nanoparticles. Measurements

dx.doi.org/10.1021/ja110014p |*J. Am. Chem. Soc.* 2011, 133, 4889–4895

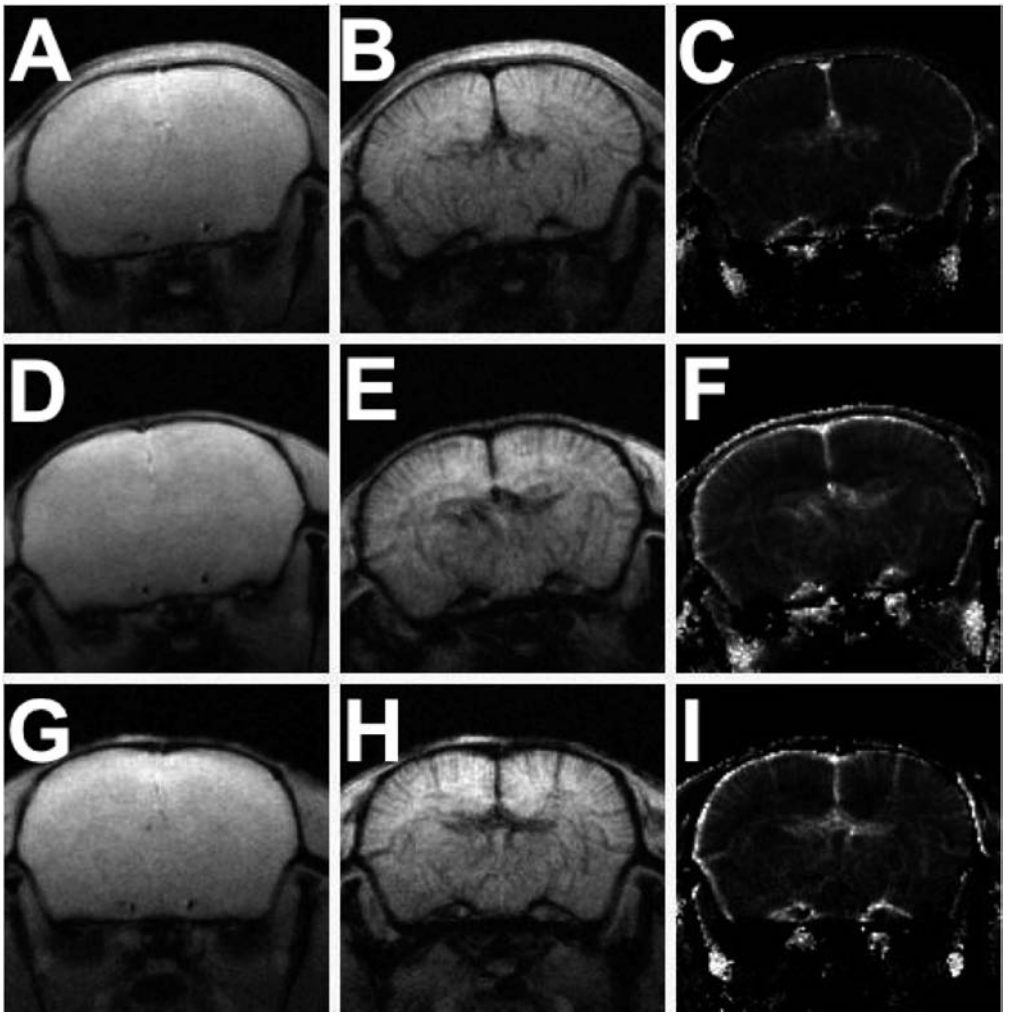

Figure 5. Representative mouse brain images acquired before and 120 s after administration of contrast agents and corresponding rCBV maps. Upper line: Precontrast (A), postcontrast (B), and rCBV map (C) obtained with APOMAG-4. Middle line: Precontrast (D), postcontrast (E), and rCBV map (F) obtained with APOMAG-6. Lower line: Precontrast (G), postcontrast (H), and rCBV map (I) obtained with Endorem.

of the transverse relaxation time (T_2) were acquired at a field of 4.7 T. The relaxivity coefficient (r_2) values, which are obtained as the slope of the plot of $1/T_2$ versus the molarity concentration of magnetic centers expressed in millimolar, were 68.5 and 102.0 mM^{-1} s^{-1} for the Apomaghemite samples of 4 and 6 nm, respectively. These r_2 values are comparable to those previously reported for the commercial contrast agent Endorem (94.8 mM^{-1} s^{-1}).[18] Figure 4 shows a representative first-passage curve obtained by plotting the signal intensity (SI) of the brain versus image acquisition time for APOMAG-6. Data have been normalized using the following relationship:

$$\text{normalized SI}\% = 100 \cdot (\text{SI}(t) - \text{SI}(0))/\text{SI}(0)$$

where SI(0) represents the average signal intensity before injection, and SI(t) is the signal intensity at time t. Quantitative comparison between the efficiency of Apomaghemite samples and Endorem was obtained by measuring the maximum signal drop. Results, reported in Table 1, show that Apomaghemite samples of both 4 and 6 nm size can induce signal drops similar to contrast agent Endorem.

To validate the efficiency of our samples in contrasting MRI images, we collected representative pre-contrast and post-contrast T_2*-weighted images acquired 120 s after injection of Apomaghemite samples and the CA Endorem, at the steady-state concentration of contrast agent in blood. Regional cerebral blood volume maps (rCBV) calculated as described in the Experimental Section are also shown. Similarly to Endorem, post-contrast images and rCBV maps obtained with Apomaghemite samples depicted very well the space arrangement of cerebral vessels. Images and maps reported in Figure 5 clearly indicate that acquiring steady-state rCBV maps using Apomaghemite samples would be comparable to Endorem.

The blood half-lives of APOMAG-4 and APOMAG-6 were estimated in anaesthetized animals by fitting the time dependence of the signal intensity in T2w images of brain with a single exponential decay according to ref 18b. Blood half-times of about 2 and 3 h were obtained for APOMAG-4 and APOMAG-6, respectively.

From the above discussion, it can be concluded that our systems can be considered as promising negative contrast agents for magnetic resonance imaging.

For the functionalization of water-soluble magnetic nanoparticles with monosaccharides ligands, we used APOMAG-4 as the starting material. The high monodispersity, the ease of apoferritin shell modification, and its high magnetic moment make this bioconjugate an ideal probe for adding new functionalities. In

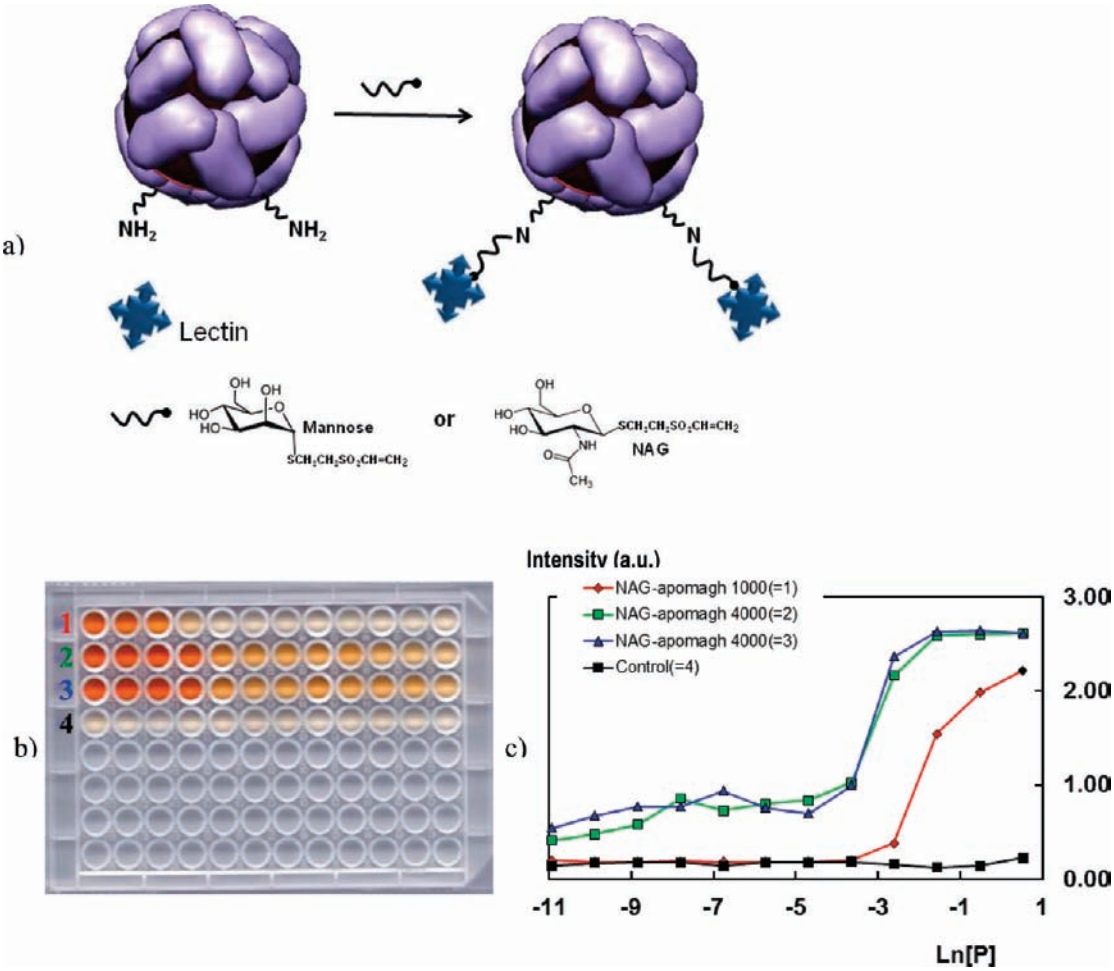

Figure 6. (a) Glycosylation of Apomaghemite nanoparticles by reaction of *N*-acetyl-D-glucosamine or D-mannose vinyl sulfone derivatives with the amine group naturally present in the Apomaghemite nanoparticles to make them recognizable by lectins. (b) Image of the ELISA plate after incubation of decreasing concentrations of the glycosylated Apomaghemite nanoparticles (left to right) with the horseradish peroxidase-lectin bioconjugate. From top to bottom, rows 1 and 2, Apomaghemite glycosylated with 1000 and 4000 mol of vinyl sulfone *N*-acetyl-D-glucosamine; row 3, duplicate of row 2 (control of reproducibility of the assay); row 4, non-glycosylated Apomaghemite nanoparticles (control of non-specific interaction Apomaghemite-lectin). (c) Quantification of the plate. Plot of the peroxidase activity of the peroxidase−lectin bioconjuate retained in the well by interaction with the nanoparticles versus concentration of nanoparticles (expressed as neperian logarithm).

fact, we have recently demonstrated that ferritin can be conjugated with different dyes or quantum dots, as a new type of dual-functional fluorescent-magnetic probe.[19] The functionalization with carbohydrates is an appealing option due to the potential of carbohydrate−protein interactions to target protein receptors at sites of localization. In particular, the presence of receptors for *N*-acetyl-D-glucosamine in hepatocytes and D- mannose receptors in liver, spleen, and alveolar macrophages encouraged us to functionalize the Apomaghemite nanoparticles with these two monosaccharides. However, the glycosylation of the protein is far from trivial.[20] In this context, we have demonstrated the versatility of the vinyl sulfone function as a general derivatization strategy for bioconjugation that leads to the reaction with the amine groups naturally present in biomolecules in mild conditions (i.e., room temperature and pH above 8).[21] Thus, the glycosylation of the Apomaghemite was addressed by reaction with vinyl sulfone derivatized *N*-acetyl-D-glucosamine and D-mannose (Figure 6a).

The synthesis of vinyl sulfone monosaccharides was carried out in two steps from the corresponding per-*O*-acetyl-1-thio-monosaccharides: The first was de-*O*-acetylation with sodium methoxide followed by treatment with divinyl sulfone (Supporting Information SI5). The recognition of the glycosylated Apomaghemite by endogenous lectins is a primary goal for its biomedical applications. The interactions between the glycosylated Apomaghemite and plant lectins were evaluated by enzyme-linked lectin assay (ELLA). Nanoparticles were fixed on an ELISA plate, and the presence of the carbohydrate moiety was revealed by incubation with horseradish peroxidase−lectins conjugates. The lectins of choice were wheat germ agglutinin (WGA) and concanavalin A (ConA) that interact with *N*-acetyl-D-glucosamine and D-mannose, respectively. As depicted in Figure 6b, glycosylation turns Apomaghemite particles into glycoproteins recognizable by plant lectins that specifically bind *N*-acetyl-D-glucosamine or D-mannose. As expected, non-glycosylated Apomaghemite (Figure 6b, row 4) is not recognized by the plant lectins. A closer analysis revealed that the two assayed concentrations of vinyl sulfone monosaccharide yielded different intensity, suggesting a different degree of glycosylation (Figure 6c). This fact is relevant because protein−carbohydrate interactions

are weak and multivalence plays a role. Thus, in the mannose receptor, like other carbohydrate-binding proteins, several individual lectin domains with weak affinity for single sugars are clustered to achieve high affinity binding to oligosaccharides.[22]

CONCLUSIONS

We have demonstrated that the pH-driven assembly−disassembly process that occurs in apoferritin is effective for the encapsulation of maghemite nanoparticles of 4 and 6 nm. The nanoparticles prepared in this way have been functionalized with two types of monosaccharides: *N*-acetyl-D-glucosamine and D-mannose vinyl sulfone derivatives. To our knowledge, this is the first example of both a templated self-assembly of apoferritin around maghemite nanoparticles and its conversion into a glycosylated specimen.

HREM, HAADF, EELS, XRD, and SQUID techniques were used to characterize the spinel phase nanocrystalline maghemite. The presence of the protein shell was revealed by negative staining, confirming the effective encapsulation of maghemite nanoparticles within the apoferritin protein shell.

The SQUID measurements confirmed the superparamagnetic behavior, required for in vivo applications, above 20 and 35 K for the 4 and 6 nm Apomaghemite samples, respectively.

MRI measurements suggested that Apomaghemite samples are promising contrast agents. Besides, Apomaghemites present added functionalities as compared to Endorem: the ease of encapsulation synthesis and the possibility of multiple functionalization thanks to the amine groups located at the external protein shell. Finally, the carbohydrate-functionalized Apomaghemite nanoparticles retained their recognition abilities, as demonstrated by the strong affinity with their corresponding carbohydrate-binding lectins.

EXPERIMENTAL SECTION

Preparation of Maghemite Colloid. Magnetite was synthesized according to Massart's method[13] by coprecipitation of Fe^{2+} and Fe^{3+} salts in stoichiometry of 0.5. By adjusting both pH (12 and 11 for 4 and 6 nm, respectively) and ionic strength (2 and 1 M $NaNO_3$ for 4 and 6 nm, respectively), the size of the resulting magnetite nanoparticles can be controlled.[12] All solutions were carefully deaerated with argon. After oxidation, a colloid of maghemite nanoparticles stable at pH 2 was obtained.

Encapsulation of Magnetic Iron Oxide Nanoparticles in Apoferritin. The pH of a 2 mL solution of Apoferritin (5 mg/mL) was slowly lowered to pH 2 with 0.1 M HCl. After being stirred for 15 min, the solution was mixed with 1 mL of a diluted nanoparticles solution of pH 2 (50 μL to 1 mL) and stirred for 30′. The pH of the resulting solution was then adjusted to 7 with 0.1 M NaOH to allow the proper subunit assembly into the 24-mer protein and then the encapsulation of nanoparticles.

The resulting clear reddish dark solution was purified to remove unfolded subunits or large nanoparticles aggregates by centrifugation (10 000 rpm, 1 h), then chromatographed on a Sephadex G-25 column to isolate the protein-containing fractions.

Glycosylation of Apomaghemite with NAG or Mannose. The purified sample (3 mL) was divided in two aliquots of 1.5 mL each (1.7×10^{-8} mol) and incubated with 1000 and 4000 mol of *N*-acetyl-D-glucosamine (NAG), respectively. After 12 h of incubation, the unreacted vinyl sulfone monosaccharide was removed by exhaustive dialysis. Next, samples were chromatographed using a Sephadex G-25 column, and the protein containing fractions were isolated. The same procedure was followed for the glycosylation of Apomaghemite with mannose.

Affinity ELISA Assay. The affinities of NAG toward WGA lectin (wheat germ agglutinin peroxidase conjugate) and mannose toward Con A (concanavalin A) lectin were evaluated by ELISA-type protocol ELLA.

Serial dilutions of the sample containing 20 μL of protein (3.3 μg/ μL) in 200 μL of 0.1 M carbonate buffer (pH 9.6) were added to the wells of an ELISA plate and adsorbed by incubation at 4 °C overnight. Wells were washed with 300 μL of PBST (3 × 3 min) and then incubated with 200 μL of horseradish peroxidase−lectin bioconjugate (0.2 μg/μL in PBST) at 37 °C for 1 h. After being washed with PBST (3 × 200 μL/3 min), the presence of lectin was detected by the peroxidase activity after stopping with 100 μL of 2 M H_2SO_4 the incubation at 37 °C for 30 min with 200 μL of 2.2 mM 1,2-phenylenediamine dihydrochloride in 0.1 M citrate buffer pH 5 with 100 μL of 2 M H_2SO_4. Quantification was carried out by measurement of the absorbance at 495 nm with a sunrise absorbance reader (Tecan).

Transmission Electron Microscopy. Electron micrographs were taken with a Philips CM-20 HR electron microscope operating at 200 keV. High-resolution electron microscopy (HREM) images were recorded using a 200 kV field emission gun electron microscope (JEM2010-FEG) with a spatial resolution of 0.19 nm at Scherzer defocus conditions. High-angle annular dark field scanning transmission microscopy (HAADF-STEM) was performed using an electron probe with a diameter of 0.5 nm at a diffraction camera length of 12 cm. EEL spectra were obtained with an energy dispersion of 0.3 eV by channel. The average particle sizes and the standard deviations were estimated from HAADF images analysis of 100 particles for both samples.

Magnetic Measurements. Magnetic measurements were performed on lyophilized samples using a magnetometer (Quantum Design MPMS-XL-5) equipped with a SQUID sensor.

X-ray Diffraction (XRD). Experimental data were collected using a Bruker D8 ADVANCE diffractometer with Cu K_a radiation.

MRI Measurements. MRI measurements were performed with a 4.7T Biospec Tomograph System (Bruker, Karlsruhe, Germany) operating at 200 MHz and equipped with a 33 cm bore magnet (Oxford Ltd., UK). Samples containing Apomaghemite nanoparticles at different iron concentrations were prepared and inserted in a 7.2 cm i.d. birdcage coil. The values of the transversal relaxation time T_2 of each sample were measured by using the standard SPIN-ECHO MULTI-ECHO sequence with the following parameters: TR/TE = 2000/15 ms, 8 echoes, FOV = 4 × 8 cm^2, MTX = 256 × 128, slice thickness = 2 mm.

In Vivo Experiments. In vivo experiments were performed to characterize the performances of Apomaghemite samples as contrast agents for mapping of cerebral blood volume (CBV) and cerebral blood flow (CBF) and were compared to Endorem. Quantitative evaluations of CBF and CBV can be performed by the bolus tracking method. Regional CBV (rCBV) can be also measured using blood pool contrast agents, at the steady-state concentration of contrast agent in blood, by acquiring T_2^* images before and after contrast agent injection and using the following relationship:

$$\mathrm{rCBV} = k \cdot \ln(\mathrm{SI\ pre}/\mathrm{SI\ post})$$

where k is a constant depending on instrumental parameters, and SI pre and SI post are the values of the signal intensity of brain before and after contrast agent injection.

In the in vivo experiments, a total of 15 Balb-c mice weighing about 20 g, five animals for each contrast agent, were used. Contrast agents were administered through the tail vein at the dosage of 23.5 mg Fe/kg.

First-passage images were acquired using an EPI sequence with the following parameters: MTX = 128 × 128, FOV = 25 × 25 mm^2, slice thickness = 2 mm, 4 EPI shots, TR/TE = 25/6.5 ms, NEX = 4 (time resolution of 5 images/s). Images were continuously recorded for 60 s. Steady-state images were acquired before and 2 min after injection of the

contrast agent using a Gradient Echo sequence with the following parameters: TR/TE = 130/6 ms, flip angle = 30°, MTX = 256 × 256, FOV = 25 × 25 mm^2 (corresponding to 0.098 × 0.098 mm^2 in-plane resolution), slice thickness = 1 mm, NEX = 4. The acquisition time for a single image was 133 s. A phantom containing 1 mM Gd-DTPA in saline was inserted in the field of view and used to normalize possible spectrometer drifts during the acquisition.

■ ASSOCIATED CONTENT

Supporting Information. A detailed description of purification (SI1) and structural characterization (SI2, SI3, and SI4) of Apomaghemites samples, as well as detailed synthesis and characterization of the vinyl sulfone derivatized carbohydrates. This material is available free of charge via the Internet at http://pubs.acs.org.

■ AUTHOR INFORMATION

Corresponding Author
josema@ugr.es; ngalvez@ugr.es

■ ACKNOWLEDGMENT

We are grateful to the MEC (project CTQ2009-09344), Junta de Andalucía project (FQM-02525), and EU I3 Project ESTEEM (contract no. 026019 RII3) for financial support.

■ REFERENCES

(1) (a) Cheon, J.; Lee, J. H. *Acc. Chem. Res.* **2008**, *41*, 1630–1640. (b) Dobson, J. *Nat. Nanotechnol.* **2008**, *3*, 139–143. (c) Jun, Y. W.; Seo, J. W.; Cheon, J. *Acc. Chem. Res.* **2008**, *41*, 179–189. (d) Campbell, R. B. *Nanomedicine* **2007**, *2*, 649–652.

(2) (a) Kettering, M.; Winter, J.; Zeisberger, M.; Streck, S. B.; Oehring, H.; Bergemann, C.; Alexxiou, C.; Hergt, R.; Halbhuber, K. J.; Kaiser, W. A.; Hilger, I. *Nanotechnology* **2007**, *18*, 175101–175110. (b) Hergt, R.; Hiergeist, R.; Zeisberger, M.; Glockl, G.; Weitschies, W.; Ramirez, L. P.; Hilger, I.; Kaiser, W. A. *J. Magn. Magn. Mater.* **2004**, *280*, 358–368. (c) Weissleder, R.; Moore, A.; Mahmood, U.; Bhorade, E.; Benveniste, H.; Chiocca, E. A.; Basilion, J. P. *Nat. Med.* **2000**, *6*, 351–354.

(3) (a) Mornet, S.; Vasseur, S.; Grasset, F.; Duguet, E. *J. Mater. Chem.* **2004**, *14*, 2161–2175. (b) Di Marco, M.; Sadun, C.; Port, M.; Guilbert, I.; Couvreur, P.; Dubernet, C. *Int. J. Nanomed.* **2007**, *2*, 609–622. (c) Corot, C.; Robert, P.; Idee, J. M.; Port, M. *Adv. Drug Delivery Rev.* **2006**, *58*, 1471–1504. (d) Laurent, S.; Forge, D.; Port, M.; Roch, A.; Robic, C.; Elst, L. V.; Muller, R. N. *Chem. Rev.* **2008**, *108*, 2064–2110.

(4) (a) Gálvez, N.; Sánchez, P.; Domínguez-Vera, J. M. *Dalton Trans.* **2005**, 2492–2495. (b) Clemente-León, M.; Coronado, E.; Soriano-Portillo, A.; Gálvez, N.; Domínguez-Vera, J. M. *J. Mater. Chem.* **2007**, *17*, 49–51. (c) Domínguez-Vera, J. M.; Gálvez, N.; Sánchez, P.; Mota, A. J.; Trasobares, S.; Hernández, J. C.; Calvino, J. J. *Eur. J. Inorg. Chem.* **2007**, 4823–4826. (d) Ueno, T.; Suzuki, M.; Goto, T.; Matsumoto, T.; Nagayama, K.; Watanabe, Y. *Angew. Chem., Int. Ed.* **2004**, *43*, 2527–2530. (e) Uchida, M.; Klem, M. T.; Allen, M.; Flenniken, M. L.; Gillitzer, E.; Varpness, Z.; Suci, P.; Young, M. J.; Douglas, T. *Adv. Mater.* **2007**, *19*, 1025–1042. (f) Gálvez, N.; Fernández, B.; Sánchez, P.; Cuesta, R.; Ceolín, M.; Clemente-León, M.; Trasobares, S.; López-Haro, M.; Calvino, J. J.; Stéphan, O.; Domínguez-Vera, J. M. *J. Am. Chem. Soc.* **2008**, *130*, 8062–8068.

(5) (a) Chen, C.; Daniel, M. C.; Quinkert, Z. T.; De, M.; Stein, B.; Bowman, V. D.; Chipman, P. R.; Rotello, V. M.; Kao, C. C.; Dragnea, B. *Nano Lett.* **2006**, *6*, 611–615. (b) Huang, X.; Bronstein, L. M.; Retrum, J.; DuFort, C.; Tsvetkova, I.; Aniagyei, S.; Stein, B.; Stucky, G.; McKenna, B.; Remmes, N.; Baxter, D.; Kao, C. C.; Dragnea, B. *Nano Lett.* **2007**, *7*, 2407–2416. (c) Dixit, S. K.; Goicochea, N. L.; Daniel, M. C.; Murali, A.; Bronstein, L.; De, M.; Stein, B.; Rotello, V. M.; Kao, C. C.; Dragnea, B. *Nano Lett.* **2006**, *6*, 1993–1999.

(6) (a) Webb, B.; Frame, J.; Zhao, Z.; Lee, M. L.; Watt, G. D. *Arch. Biochem. Biophys.* **1994**, *309*, 178–183. (b) Aime, S.; Frullano, L.; Geninatti Crich, S. *Angew. Chem., Int. Ed.* **2002**, *41*, 1017–1019. (c) Simsek, E.; Kilic, M. A. *J. Magn. Magn. Mater.* **2005**, *293*, 509–513. (d) Colacio, E.; Domínguez-Vera, J. M. *Inorg. Chem.* **2003**, *42*, 6983–6985.

(7) Swift, J.; Butts, C. A.; Cheung-Lau, J.; Yerubandi, V.; Dmochowski, I. J. *Langmuir* **2009**, *25*, 5219–5225.

(8) (a) Zhang, H.; Ma, Y.; Sun, X. L. *Med. Res. Rev.* **2010**, *30*, 270–289. (b) Seeberger, P. H.; Werz, D. B. *Nature* **2007**, *446*, 1046–1051. (c) Park, S.; Lee, M. R.; Shin, I. *Chem. Soc. Rev.* **2008**, *37*, 1579–1591.

(9) Lis, H.; Sharon, N. *Chem. Rev.* **1998**, *98*, 637–674.

(10) (a) de la Fuente, J. M.; Penadés, S. *Biochem. Biophys. Acta* **2006**, *1760*, 636–651. (b) Lartigue, L.; Oumzil, K.; Guari, Y.; Larionova, J.; Guérin, C.; Montero, J. L.; Barragan-Montero, V.; Sangregorio, C.; Caneschi, A.; Innocenti, C.; Kalaivani, T.; Arosio, P.; Lascialfari, A. *Org. Lett.* **2009**, *11*, 2992–2995. (c) Earhart, C.; Jana, N. R.; Erathodiyil, N.; Ying, J. Y. *Langmuir* **2008**, *24*, 6215–6219. (d) El-Boubbou, K.; Gruden, C.; Huang, X. *J. Am. Chem. Soc.* **2008**, *129*, 13392–13393. (d) Liu, L. H.; Dietsch, H.; Schurtenberger, P.; Yan, M. *Bioconjugate Chem.* **2009**, *20*, 1349–1355. (e) Liang, C. H.; Wang, C. C.; Lin, Y. C.; Chen, C. H.; Wong, C. H.; Wu, C. Y. *Anal. Chem.* **2009**, *81*, 7750–7756.

(11) Lu, A. H.; Salabas, E. L.; Schüth, F. *Angew. Chem., Int. Ed.* **2007**, *46*, 1222–1244.

(12) Vayssières, L.; Chanéac, C.; Tronc, E.; Jolivet, J. P. *J. Colloid Interface Sci.* **1998**, *205*, 205–212.

(13) Massart, R. *IEEE Trans. Magn.* **1981**, 1247–1248.

(14) (a) Mann, S.; Archibald, D. D.; Didymus, J. M.; Douglas, T.; Heywood, B. R.; Meldrum, F. C.; Reeves, N. J. *Science* **1993**, *261*, 1286–1292. (b) Wong, K. K. W.; Douglas, T.; Gider, S.; Awschalom, D. D.; Mann, S. *Chem. Mater.* **1998**, *10*, 279–285. (c) Meldrum, F. C.; Heywood, B. R.; Mann, S. *Science* **1992**, *257*, 522–523.

(15) http://www2.uca.es/dept/cmat_qinor/catalisis/tem-uca-server.htm.

(16) Tronc, E.; Fiorani, D.; Nogués, M.; Testa, A. M.; Lucari, F.; D'Orazio, F.; Grenèche, J. M.; Wernsdorfer, W.; Galvez, N.; Chanéac, C.; Mailly, D.; Jolivet, J. P. *J. Magn. Magn. Mater.* **2003**, *262*, 6–14.

(17) (a) Hyeon, T.; Lee, S. S.; Park, J.; Chung, Y.; Na, H. B. *J. Am. Chem. Soc.* **2001**, *123*, 12798–12801. (b) Jun, Y.; Huh, Y. M.; Choi, J. S.; Lee, J. H.; Song, H. T.; Kim, S. J.; Yoon, S.; Kim, K. S.; Shin, J. S.; Suh, J. S.; Cheon, J. *J. Am. Chem. Soc.* **2005**, *127*, 5732–5733.

(18) (a) Masotti, A.; Pitta, A.; Ortaggi, G.; Corti, M.; Innocenti, C.; Lascialfari, A.; Marinone, M.; Marzola, P.; Daducci, A.; Sbarbati, A.; Micotti, E.; Orsini, F.; Poletti, G.; Sangregorio, C. *Magn. Reson. Mater. Phys.* **2009**, *22*, 77–87. (b) Schwarz, A. J.; Reese, T.; Gozzi, A.; Bifone, A. *Magn. Reson. Imaging* **2003**, *21*, 191–200.

(19) (a) Fernandez, B.; Galvez, N.; Sanchez, P.; Morales, J.; Santoyo, F.; Cuesta, R.; Dominguez-Vera, J. M. *Inorg. Chim. Acta* **2007**, *360*, 3951–3954. (b) Fernández, B.; Gálvez, N.; Cuesta, R.; Hungría, A. B.; Calvino, J. J.; Domínguez-Vera, J. M. *Adv. Funct. Mater.* **2008**, *18*, 3931–3935.

(20) (a) Davis, B. G. *Chem. Rev.* **2002**, *102*, 579–601. (b) Gamblin, D. P.; Scanlan, E. M.; Davis, B. G. *Chem. Rev.* **2009**, *109*, 131–163.

(21) (a) Lopez-Jaramillo, F. J.; Perez-Banderas, F.; Hernandez-Mateo, F.; Santoyo-Gonzalez, F. *Acta Crystallogr., Sect. F* **2005**, *61*, 435–438. (b) Morales-Sanfrutos, J.; Lopez-Jaramillo, J.; Ortega-Muñoz, M.; Megia-Fernandez, A.; Perez-Balderas, F.; Hernandez-Mateo, F.; Santoyo-Gonzalez, F. *Org. Biomol. Chem.* **2010**, *8*, 667–678.

(22) Taylor, M. E.; Benzouška, K.; Drickamer, K. *J. Biol. Chem.* **1992**, *267*, 1719–172.